

PACS numbers: 87.19.Uv; 42.55.Px; 42.62.Be
DOI: 10.1070/QE2002v032n11ABEH002331

Arterial pulse shape measurement using self-mixing effect in a diode laser

Jukka Hast, Risto Myllyla, Hannu Sorvoja, Jari Miettinen

Abstract. **The self-mixing effect in a diode laser and the Doppler technique are used for quantitative measurements of the cardiovascular pulses from radial arteries of human individuals. 738 cardiovascular pulses from 10 healthy volunteers were studied. The Doppler spectrograms reconstructed from the Doppler signal, which is measured from the radial displacement of the radial artery, are compared to the first derivative of the blood pressure signals measured from the middle finger by the Penaz technique. The mean correlation coefficient between the Doppler spectrograms and the first derivative of the blood pressure signals was 0.84, with a standard deviation of 0.05. Pulses with the correlation coefficient less than 0.7 were neglected in the study. Percentage of successfully detected pulses was 95.7 %. It is shown that cardiovascular pulse shape from the radial artery can be measured noninvasively by using the self-mixing interferometry.**

Keywords: *self-mixing interferometry, diode laser, Doppler signal, cardiovascular pulse shape, blood pressure.*

1. Introduction

The shape and rhythm of the cardiovascular pulsations are traditional indicators of cardiovascular diseases. Small and weak pulses may indicate heart failure, hypovolemia or severe aortic stenosis. Large and bounding pulses may be a sign of fever, anaemia, hyperthyroidism, aortic regurgitation, bradycardia, heart block or atherosclerosis. Bisferiens pulses, which are characterised by an increased amplitude and a double systolic peak, might be due to aortic regurgitation, aortic stenosis and regurgitation or hypertropic cardiomyopathy [1]. Several other types of abnormal cardiovascular pulses can be also categorised and more detailed description of them can be found in book [2]. From this point of view, a sensor that can measure the pulse shape accurately has high potential for applications in the field of medical diagnosis.

The radial artery in the wrist offers a convenient place for pulse measurements because this artery is close to skin surface and thus, a pulse can be easily detected. In addition, the wrist bone under the artery offers a good mechanical support for the sensor. Easy access to cardiovascular pulsations has been widely exploited to study heart rate and blood pressure in the wrist, and many different sensor types have been used. Pulse detection in heart rate and blood pressure measurements have been done with piezoelectric [3], strain gauge differential pressure [4], optical [5], and fibreoptic sensors [6]. Recently, sensors based on an electromechanical film (EMF) and polyvinylidene fluoride (PVDF) have been used for radial artery pulse detection [7, 8].

The laser Doppler technique serves as a good basis for an alternative sensor type to detect cardiovascular pulsations, because it offers a very accurate method to measure the movement of the arterial wall. The technique is widely used in the biomedical optics to blood flow measurements. It was used for cardiovascular pulsations detection from different arteries of human body [9] and pulse parameters detection using self-mixing interferometry [10].

The development of laser Doppler technique was initiated in 1960s. Four years after the invention of a laser in 1960, the method was proposed for measuring the velocity of particles in solutions by the Doppler shift of light [11]. Laser Doppler velocimetry (LDV), which uses the Doppler shift of laser light as the information carrier, was first introduced to the flow measurement of red blood cells in a glass tube [12] and then a few years later it was used for blood perfusion measurement in the microcirculation [13]. Since then a number of clinical and experimental applications of laser Doppler technique in biomedical optics has been done in laser Doppler flowmetry (LDF) [14, 15], laser Doppler microscopy [16], perfusion imaging [17], and biotissue vibration measurement by laser and speckle interferometry [18].

The optical interferometer, needed in a laser Doppler apparatus, can be constructed in several ways. The most common are devices based on Michelson or Mach–Zehnder interferometers. Another possible way is to use the effect of self-mixing in a laser cavity. In the self-mixing effect, backscattered light from the probed object is coupled back into the laser cavity, where it interacts with the original light. If the appropriate conditions are fulfilled, the interference occurs, and it is detected with a photodetector located at

Jukka Hast, Risto Myllyla, Hannu Sorvoja University of Oulu, Department of Electrical Engineering, Optoelectronics and Measurements Laboratory, PO BOX 4500, 90014 University of Oulu, Oulu Finland; tel.: +358 8 553 2756, fax. +358 8 553 2774, e-mail: jukka.hast@ee.oulu.fi; http://www.ee.oulu.fi/EE/OEM.Laboratory/index.shtml;
Jari Miettinen Polar Electro Oy, Professorintie 5, 90440 Kempele, Finland; http://www.polar.fi

Received 28 August 2002
Kvantovaya Elektronika **32** (11) 975–980 (2002)]
Submitted in English

the opposite side of the laser cavity. The phenomenon was first discovered by King and Steward, who noticed that external feedback to laser cavity induces intensity modulation in the output of a gas laser [19]. A few years later, the first laser Doppler velocimeter, where laser cavity was used as an optical mixer, was presented [20]. Self-mixing interferometry was exploited by many research teams to develop different measurement applications in velocimetry [21], displacement and distance measurements [22], ranging [23], 3D-imaging [24] and laser processing of materials [25]. It has been also applied in biomedical optics to blood flowmetry [26], skin vibration measurements due to mechanomyogram [27], pulse wave velocity (PWV) measurements [28], baroreflex regulation [29], and arterial compliance measurements [30].

The self-mixing effect occurs not only in lasers, but also in low-coherence light sources like superluminescent diodes (SLD), that serve as a light source in low-coherence interferometers [31].

In this paper, we use the laser Doppler technique based on self-mixing effect in a diode laser to measure the shape of the arterial pulse from radial artery. The arterial pulse shape reconstructed from the Doppler signal is proportional to the first derivative of the blood pressure pulse. For reference, blood pressure is also detected from the middle finger using a commercial blood pressure monitor. A similarity between the arterial pulse shape from radial artery and middle finger is quantified by calculating the correlation coefficients for each pulse. Measurements were performed with 10 healthy volunteers, and totally 738 pulses were analysed.

2. Materials and methods

2.1 Principle of operation of a laser Doppler device based on the self-mixing effect in a diode laser

The laser Doppler technique is based on the relation where scattered light from the moving target contains a frequency shift that is proportional to the velocity of the moving target:

$$f_{\mathrm{D}} = \frac{2nv_{\mathrm{s}}}{\lambda}\cos\theta. \tag{1}$$

Here, f_{D} is the measured Doppler beat frequency produced by optical mixing of the original and scattered laser light. The refractive index of the medium is n. In our case, the device operates in air, and thus $n = 1$. The velocity of the moving target is v_{s} and λ is the emission wavelength of the diode laser. The angle between the velocity vector of the target and laser beam wave vector is θ. In the pulse shape measurements, the laser beam is pointed towards radial artery, and radial displacement of the arterial wall is perpendicular to the laser beam, so that $\cos\theta = 1$. Thus, Eqn (1) is reduced to

$$f_{\mathrm{D}} = \frac{2v_{\mathrm{s}}}{\lambda}.$$

Furthermore, v_{s} corresponds to the radial velocity of the arterial wall, which is related to the velocity of the blood pressure change, i.e., to the first derivative $\mathrm{d}P/\mathrm{d}t$ of the blood pressure.

The self-mixing effect can be simulated with the help of a three-mirror Fabry–Perot structure, as shown in Fig. 1. Laser mirrors (*1*) and (*2*) enclose the laser cavity of length L with the effective refractive index μ_{eff}. The external target (*3*) is located on the optical axis z at the distance L_{ext}, which is the length of the external cavity. The external target in this case is the radial artery. (*4*) is a monitor photodiode employed to detect the power fluctuations behind the laser cavity.

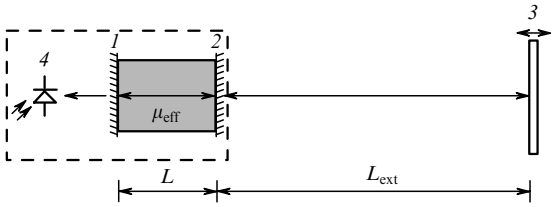

Figure 1. Schematic arrangement of self-mixing effect in a diode laser.

The use of semiconductor lasers enables the construction of interferometers that are small in size, inexpensive, and accurate. Moreover, the setup is simple, since there is only one optical axis to control. The theory concerning the self-mixing effect can be found in [32] and here we present only basic equations. When an external target moves along the optical axis, the change ΔP in the laser output caused by the optical feedback can be written as [33]

$$\Delta P \approx g_{\mathrm{c}} - g_{\mathrm{th}} = -\frac{\kappa}{L}\cos\left[2\pi f\left(\tau_{\mathrm{ext}} + \frac{2v_{\mathrm{s}}t}{c}\right)\right], \tag{2}$$

where g_{c} and g_{th} are the threshold gains with and without the external feedback, respectively, $\tau_{\mathrm{ext}} = 2L_{\mathrm{ext}}/c$ is the round-trip time of light propagation in the external cavity, c is the speed of light, and f is the laser emission frequency. The coupling factor $\kappa = r_{2\mathrm{ext}}(1 - |r_{2\mathrm{s}}|^2)/r_{2\mathrm{s}}$, where $r_{2\mathrm{s}}$ is the amplitude reflection coefficient of laser mirror (*2*) and $r_{2\mathrm{ext}}$ is the amplitude reflection coefficient of the external targer (*3*). Because the velocity v_{s} of the moving target is related to the Doppler shift according to Eqn (1), the power fluctuations in Eqn (2) contain information on the velocity.

The strength of external feedback is an important consideration in self-mixing interferometers. The feedback parameter C_{fb} is defined as

$$C_{\mathrm{fb}} = \frac{\tau_{\mathrm{ext}}}{\tau_{\mathrm{las}}}\kappa\left(1 + \alpha^2\right)^{1/2}, \tag{3}$$

where $\tau_{\mathrm{las}} = 2L/c$ is the round-trip delay in the laser cavity. α is the laser linewidth enhancement factor, which is the ratio of the real and imaginary parts of the variation in the complex refractive index of the active medium with its density [30]. If the parameter $C_{\mathrm{fb}} \ll 1$, power fluctuations at the laser output are sinusoidal. When C_{fb} increases, the fluctuations become more saw-tooth-like. When $C_{\mathrm{fb}} > 1$, the operation of the laser is no longer stable, leading to increased noise and mode hopping [34].

2.2 Measurement system

The block diagram of the measurement system is shown in Fig. 2. The system comprises a self-mixing interferometer in a laser Doppler probe, where also a transimpedance preamplifier is located. During the measurement, the probe is attached above the radial artery, as shown in

Fig. 2. The self-mixing interferometer is capable of measuring a displacement of 150 μm with an accuracy of 1 μm on a highly scattering surface like paper or skin. By using appropriate optical elements between the interferometer and the target, this distance can be increased to 250 μm [35]. The PC-interface card contains main amplifiers, a Doppler laser diode driver, and a software-controlled filter block. The data acquisition card collects the measured data and saves them to the computer hard disk. Finally, data processing and analysis are performed with a PC-interface card.

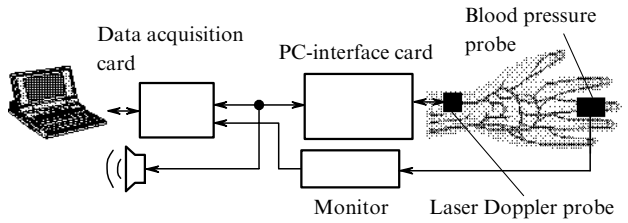

Figure 2. Block diagram of the measurement system.

Comparative blood pressure measurements are performed with a Finapres Ohmeda 2300 finger blood pressure monitor operating on the basis of the so-called Penaz technique, according to which the externally applied pressure is kept equal to the arterial pressure during whole cardiac cycle. The arterial walls are unloaded because of zero transmural pressure, the size of the arteries is not changed, and the blood volume remains constant. The blood volume is measured with a photopletysmograph, and the analog output of the device is scaled so that 1 V equals to 100 mmHg.

Data processing of the measured blood pressure and the Doppler signal follows the flow chart shown in Fig. 3. After analogue-to-digital conversion and storing to disk, signals are timed to each other, because of a time delay of about 20 to 40 ms between locations of the Doppler probe and the blood pressure probe. Then, the blood pressure signal is differentiated to obtain the signal proportional to the velocity dP/dt of the pressure change. The Doppler spectrogram is reconstructed from the Doppler signal by calculating fast Fourier transform (FFT) with 512 points per signal sample. After these operations, the data corresponding to each pulse are picked out from the data vectors and stored to a pulse matrix, where each column contains data for single arterial pulse. Before calculating the cross correlation between the pulses of the derivative of blood pressure and the Doppler spectrogram, each pulse on both matrixes is zero averaged and normalised. The cross correlation coefficients, X_{corr}, are calculated for each pulse using the equation [36]

$$X_{\mathrm{corr}}(n) = \frac{r_{xy}(n) r_{xy}(n)}{|r_{xx}(0) r_{yy}(0)|^{1/2}}, \tag{4}$$

where $r_{xy}(n)$ is the estimate of the cross-covariance defined as

$$r_{xy}(n) = \begin{cases} \dfrac{1}{N} \displaystyle\sum_{k=0}^{N-n-1} x(k) y(k+n), & n = 0, 1, 2, \ldots, N, \\ \dfrac{1}{N} \displaystyle\sum_{k=0}^{N+n-1} x(k-n) y(k), & n = 0, -1, -2, \ldots, N; \end{cases}$$

$$r_{xx}(0) = \frac{1}{N} \sum_{k=0}^{N-1} [x(k)]^2; \quad r_{yy}(0) = \frac{1}{N} \sum_{k=0}^{N-1} [y(k)]^2;$$

N is the length of two sequences $x(k)$ and $y(k)$. The pulse shape reconstructed from the Doppler spectrogram corresponds to $x(k)$, and the pulse shape from dP/dt corresponds to $y(k)$, respectively. At the last stage of the experiment with each volunteer, the mean values, $\langle X_{\mathrm{corr}} \rangle$, and standard deviations, σ_{std}, for all measured pulses are calculated using equations

$$\langle X_{\mathrm{corr}} \rangle = \frac{1}{m} \sum_{j=1}^{m} X_{\mathrm{corr}}^{j}, \quad \sigma_{\mathrm{std}} = \left[\frac{1}{m} \sum_{j=1}^{m} \left(X_{\mathrm{corr}}^{j} - \langle X_{\mathrm{corr}} \rangle \right)^2 \right]^{1/2},$$

where m is the number of pulses and X_{corr}^{j} is the correlation coefficient for the jth pulse.

2.3 Correlation between the blood pressure pulse shape and the Doppler spectrogram

Typical cardiovascular pulses measured from the middle finger with the blood pressure monitor and from the radial artery with the self-mixing interferometer are demonstrated in Fig. 4. The blood pressure pulse and its first derivative from the middle finger are shown in Figs 4a and b. The measured Doppler signal from the radial movement of the

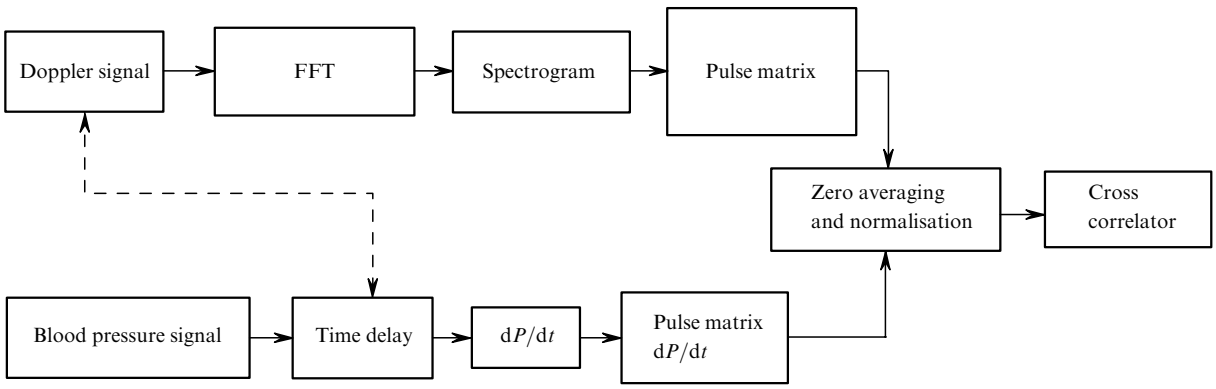

Figure 3. Flow chart of the data processing sequence.

radial artery and its reconstructed Doppler spectrogram are shown in Figs 4c and d. Because the Doppler frequency is proportional to the radial velocity of the radial artery wall, the shapes of the Doppler spectrogram and the derivative of the blood pressure pulse are similar. Here, the change in the shape of the blood pressure pulse during its propagation from the wrist to the middle finger is neglected.

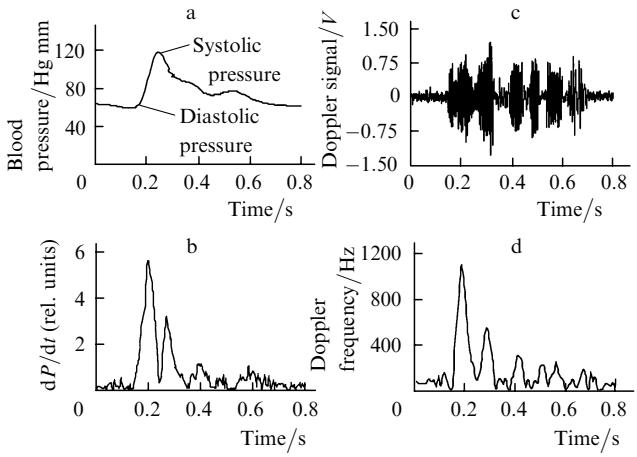

Figure 4. Blood pressure pulse from the middle finger (a); calculated first derivative of the blood pressure pulse (b); Doppler signal from the movement of the radial artery during the same pulse (c); and reconstructed spectrogram from the Doppler signal (d).

A strong peak in Figs 4b and d can be attributed to the rising edge of the blood pressure pulse. The maximum Doppler frequency at the rising edge reaches approximately 1100 ± 0.45 Hz, which corresponds to the radial velocity of 445 ± 0.18 μm s^{-1}. Here, the accuracy is limited by temperature stabilisation of the laser, which is $\pm 1\,^{\circ}C$. For comparison, in reference paper [9], a radial velocity of 350 μm s^{-1} for the radial artery was measured.

The radial displacement of the radial artery can be determined by integrating the velocity diagram over time on the rising edge of the blood pressure pulse using the trapezoidal integration method in the time limits from 0.15 to 0.25 s. This integration yields for the radial displacement of the radial artery a value of 56 ± 1 μm.

On the falling edge, the peak is approximately halved. The corresponding peaks around 0.4 and 0.6 s can be found also in Figs 4b and d. However, the Doppler spectrogram contains some extra peaks, for example, in the interval from 0.6 to 0.8 s, which are due to skin vibration. Their frequency components are between 100 and 200 Hz. In this case, the correlation coefficient during the whole pulse between the derivative of the blood pressure pulse and the Doppler spectrogram equals to 0.89. This indicates that there is a strong correlation between the shapes of the Doppler spectrogram and dP/dt.

3. Measurement results

We performed measurements with a group of 10 healthy young male volunteers, whose average age was 26 years. The blood pressure signal was recorded from the right hand's middle finger using a blood pressure monitor. The radial displacement above the right hand's radial artery was measured using the self-mixing interferometer, which was carefully placed above the artery. During the measurement, each volunteer sat relaxed in a chair and his hands were placed to the heart level. The duration of each measurement was 60 s, and totally 738 cardiovascular pulses were recorded.

Signals measured from a volunteer during 30 s are shown in Fig. 5. The curve in Fig. 5a exhibits low-frequency (~ 0.1 Hz) variations in the amplitude of the blood pressure pulses, which correspond to the baroreflex part of the autonomic regulation. The baroreflex controls the blood pressure and maintains its normal level despite variations in physical stress of a human individual.

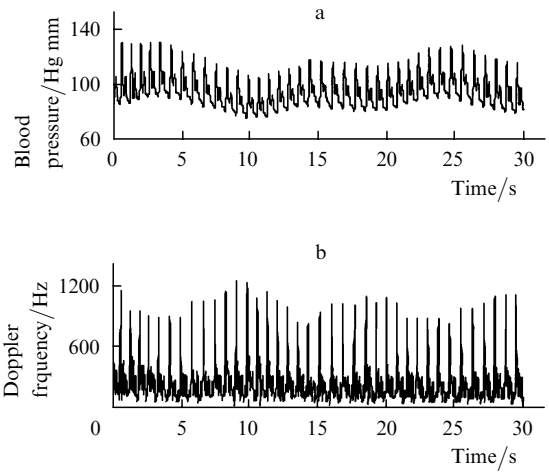

Figure 5. Blood pressure pulse signal (a) and Doppler spectrogram (b) from a volunteer during a 30-second measurement.

The Doppler spectrogram, shown in Fig. 5b, also has same amplitude variations, but in this case they seem to be in an inverse phase compared to those of the blood pressure. It can be explained by the variations in the elasticity of the arterial wall. At higher pressure, the arterial wall is in a more strained state than at lower pressure. This change in the strain affects the movement of the arterial wall and can be detected with a self-mixing interferometer. Thus, the pressure pulse amplitude variations affect the measured Doppler signal. Monitoring of baroreflex regulation by means of self-mixing interferometry was discussed in more detail in the reference paper [27].

Measurement results for all 10 volunteers are presented in Table 1. For each volunteer age, the average blood

Table 1.

Volunteer number	Age	Blood pressure/Hg mm		Number of pulses	$\langle X_{corr} \rangle$	σ_{std}
		Systolic	Diastolic			
1	27	133	80	77	0.80	0.07
2	25	126	77	75	0.85	0.05
3	27	122	70	78	0.83	0.05
4	29	131	81	75	0.84	0.05
5	21	115	75	80	0.87	0.04
6	32	121	82	67	0.77	0.10
7	26	125	79	65	0.81	0.07
8	25	110	65	71	0.86	0.05
9	22	132	85	76	0.86	0.04
10	28	121	76	74	0.82	0.05

pressure, $\langle$*Blood pressure*$\rangle$, from whole measurement, the number of pulses in the measurement, the cross correlation coefficient, $\langle X_{\mathrm{corr}} \rangle$ between the first derivative of the blood pressure pulse and the Doppler spectrogram during the measurement sequence are presented. In the last column, the standard deviation of the correlation coefficient, $\langle \sigma_{\mathrm{std}} \rangle$, during each measurement is shown.

Fig. 6 presents correlation coefficients for all 738 pulses, which were measured. The mean value of 0.83 is shown as a solid line. One can see that most of the values are around the average. However, in some pulses the correlation coefficients are lower than 0.7.

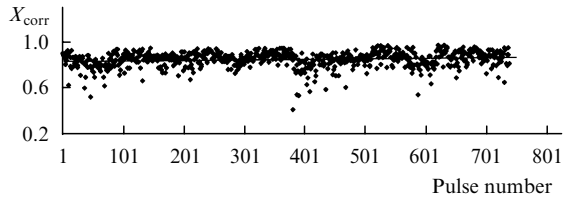

Figure 6. Correlation coefficient for all measured pulses. The average value is shown with a solid line.

The case of the very low correlation between the derivative of the blood pressure pulse and the Doppler spectrogram, corresponding to the pulse No. 47 in Fig. 6, is demonstrated in Fig. 7. The normalised derivative of the blood pressure pulse is shown in Fig.7a, and the corresponding normalised Doppler spectrogram is shown in Fig. 7b. One can see that the Doppler spectrogram contains extra peaks above time interval of 0.25 s compared to the derivative of blood pressure pulse. In this case, the correlation between signals is only 0.51. This is due to the external artifacts during the measurement sequence, which distorts the Doppler signal. The artifacts are easily generated because of high sensitivity of the interferometer to the movement. For correct evaluation of the Doppler spectrogram, the decision that the pulse detection is misread should be made if the correlation coefficient is less than 0.7. This limit was selected empirically comparing the shapes of the signals.

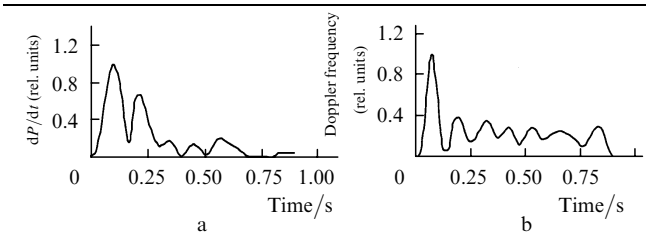

Figure 7. Normalised first derivative of the blood pressure signal (a) and the corresponding normalised Doppler spectrogram (b) from the pulse No. 47, for which $X_{\mathrm{corr}} = 0.51$.

The number of pulses, for which $X_{\mathrm{corr}} < 0.7$ is 32 of total number of 738 detected pulses. This means that 95.7 % of the pulses were detected successfully. However, this has a small effect on the total correlation coefficient and the standard deviation. When the pulses, whose correlation coefficient is less than 0.7, are not accounted for, the correlation coefficient increases to 0.84 and the standard deviation decreases to 0.05.

The mean correlation coefficient $\langle X_{\mathrm{corr}} \rangle$ between the first derivative of the blood pressure pulse and the Doppler spectrogram for the corresponding pulses was above 0.8 for all volunteers except for the volunteer number 6. The mean standard deviation σ_{std} for them was also less than 0.1 except for the volunteer No. 6. Fig. 8 shows how the correlation coefficient changes during the measurement sequence for volunteer No. 4, (Fig. 8a), and the volunteer No. 6, (Fig. 8b). In the case of volunteer No. 4, the correlation coefficient varies around the mean value, which is shown with solid line. However, in the case of volunteer No. 6, the average value of the correlation coefficient decreases during the measurement sequence. Here, the solid line shows the linear mean square approximation of the X_{corr} values. The decrease is due to poor attachment and positioning of the laser Doppler probe. During this measurement, the probe moved and this caused the decreasing trend of the correlation coefficient. This problem was encountered only with this volunteer and was included to this study just to show how a change of the laser Doppler probe position affects the correlation coefficient.

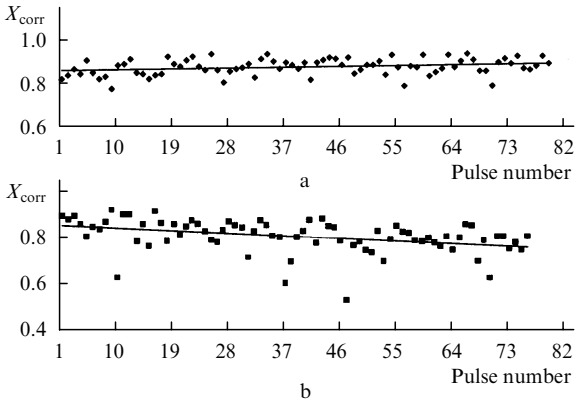

Figure 8. Alteration of the correlation coefficient during the measurements for volunteers number 4 (a) and number 6 (b).

4. Discussion

The shape of the cardiovascular pulse contains a lot of information about the state of the human body. This information can be received by means of the laser Doppler technique. We have studied the correlation between the shape of the first derivative of the blood pressure pulse measured from the middle finger and the reconstructed Doppler spectrogram from the movement of the radial artery. The radial movement of the radial artery was measured using self-mixing interferometry. The self-mixing interferometry is a challenging technique to this application because it is cheap, simple and the interferometer is compact in size and accurate.

During this study, 10 volunteers were measured and totally 738 cardiovascular pulses were analysed. The correlation between the shape of the first derivative of the blood pressure pulse and the reconstructed Doppler spectrogram was 0.84, with standard deviation of 0.05, when pulses with correlation lower than 0.7 were neglected. The percentage of successfully detected pulses was 95.7 %. The limit of 0.7 was empirically determined by comparing the shapes of the first derivative of the blood pressure pulses and the corresponding reconstructed Doppler spectrograms to each other.

Although the self-mixing interferometry is an accurate method for the pulse shape measurements, it has also some disadvantages. Because of high sensitivity of the interferometer to the movement, external artifacts are easily generated along with the measured Doppler signal. Typically, these artifacts cause an error, which is at the same frequency band as the information signal, and this results in misdetecting the correct shape. However, we found that the rising edge of the blood pressure can be detected from all measured pulses. The largest differences between the pulse spectrogram and the first derivative of the blood pressure arise during the falling edge of the blood pressure pulse.

5. Conclusions

Thus, according to our measurements, the pulse shape can be determined using self-mixing interferometry. Compared to the finger blood pressure measurement technique used in this study, the Doppler signal contains valuable additional information about the state of the cardiovascular system. Because it corresponds to the radial velocity of the arterial wall, the Doppler signal can be used to determine the variation of the arterial lumen by integrating the velocity vector in time. If the blood pressure is known, the variation in the arterial compliance can be measured. The arterial compliance, which is the ratio of the pressure ΔP change to the change of arterial lumen ΔA, is an important parameter for cardiovascular diagnostics. However, to do this, the internal radius of the artery should also be known, which is difficult to measure by purely optical techniques, but can be determined, e.g., by acoustic or photoacoustic methods.

Acknowledgements. The authors thank A.V. Priezzhev for valuable discussions and the language check of the paper. The first author acknowledges the financial support of the Graduate school in Electronics, Telecommunications and Automation (GETA).

References

1. Bates B. *A Guide to Physical Examination* (Philadelphia, USA: J.B. Lippingcott Company, 1995).
2. O'Rourke M.F., Kelly R.P., Avolio A.P. *The arterial pulse* (Pennsylvania, USA: Lea & Febiger, 1992).
3. Im J.J., Lessard C.S. *Proc. of IEEE-EMBC and CMBEC* (Montreal, 1995) Vol. 2, p. 1033.
4. Arimoto M., Yonezawa Y., Caldwell W.M. *Proc. of the First Joint BMES/EMBS Conf.* (Atlanta, USA, 1999) p. 693.
5. Gagnadre C., Billon M., Thuillier S. *Electron. Lett.*, **32**, 1991 (1998).
6. Dupuis P., Eugene C. *IEEE Trans. Instr. Meas.*, **49**, 498 (2000).
7. Ruha A., Miettinen J., Sorvoja H., Nissilä S. *Proc. of BIOSIGNAL'96* (Brno, Czech. Republic, 1996) p. 198.
8. Sorvoja H. *Licentiate Thesis* (University of Oulu, 1998).
9. Hong H., Fox M. *Biomed. Opt.*, **2**, 382 (1997).
10. Meigas K., Kattai R., Lass J. *Medical and Biological Engineering and Computing*, **37**, 93 (1999).
11. Cummins H.Z., Knable N., Yeh Y. *Phys. Lett.*, **12**, 150 (1964).
12. Riva C., Ross B., Benedek G.B. *Investigative Opthalmology*, **11**, 91 (1972).
13. Stern M.D. *Nature*, **254**, 56 (1975).
14. Shepherd A.P., Öberg P.A. *Laser-Doppler Blood Flowmetry* (Netherlands: Kluwer Acad. Publ., 1990).
15. Belcaro G., Hoffmann U., Bollinger A., Nicolaides A. *Laser-Doppler* (London – Los Angeles – Nicosia: Med-Orion Publ. Comp., 1994).
16. Priezzhev A.V., Stepanov A.S. *Lasers in Medicine*, **1**, 31 (1997).
17. Wardell K., Jakobsson A., Nilsson G.E. *IEEE Trans. Biomed. Eng.*, **40**, 309 (1993).
18. Ul'yanov S.S., Ryabukho V.P., Tuchin V.V. *Opt. Eng.*, **33**, 908 (1994).
19. King P.G.R., Steward G.J. *New Scientist*, **17**, 180 (1963).
20. Rudd M.J. *J. Phys. E-Scientific Instr.*, **1**, 723 (1968).
21. Shinohara S., Mochizuki A., Yoshida H., Sumi M. *Appl. Opt.*, **25**, 1417 (1986).
22. Donati S., Giuliani G., Merlo S. *IEEE J. Quantum Electron.*, **31**, 113 (1995).
23. Beheim G., Fritsch K. *Appl. Opt.*, **25**, 1439 (1986).
24. Gagnon E., Rivest J.-F. *IEEE Trans. Instr. Meas.*, **48**, 693 (1999).
25. Gordienko V.M., Dmitriev A.K., Konovalov A.N., Kurochkin N.N., Putivskii Yu.Yu., Panchenko V.Yu., Ulanov V.A. *Kvantovaya Elektron.*, **23**, 869 (1996) [*Quantum Electron.*, **26**, 846 (1996)].
26. De Mul F.F.M., Koelink M.H., Weijers A.L., Greve J., Aarnoudse J.G., Graaff R., Dassel A.C.M. *Appl. Opt.*, **31**, 5844 (1992).
27. Courteville A., Gharbi T., Cornu J.Y. *J. Biomed. Opt.*, **3**, 281 (1998).
28. Hast J., Myllylä R., Sorvoja H., Miettinen J. *Molecular and Quantum Acoustics*, **22**, 95 (2001).
29. Hast J., Myllylä R., Sorvoja H., Nissilä S. *Proc SPIE Int. Soc. Opt. Eng.*, **5251**, 232 (2001).
30. Hast J., Myllylä R., Sorvoja H., Miettinen J. *Proc SPIE Int. Soc. Opt. Eng.*, **4619**, 259 (2002).
31. Rovati L., Docchio F. *IEEE Photon. Technol. Lett.*, **10**, 123 (1998).
32. Petermann K. *Laser Diode Modulation and Noise* (Tokyo: Kluwer Acad. Publ., 1991).
33. Koelink M.H., Slot M., de Mul F.F.M., Greve J., Graaff R., Dassel A.C.M., Aarnoudse J.G. *Appl. Opt.*, **31**, 3401 (1992).
34. Acket G.A., Lenstra D., den Boef A.J., Verbeek B.H. *IEEE J. Quantum Electron.*, **20**, 1163 (1984).
35. Hast J., Myllylä R., Sorvoja H., Miettinen J. *J. Asian Phys.*, **10** (4) (2001).
36. Ifeachor E.C., Jervis B.W. *Digital Signal Processing: a Practical Approach* (USA, Addison-Wesley Publ. Comp., 1993).